Egyptian Journal of Chemistry
http://ejchem.journals.ekb.eg/

Synthesis, Anticancer Activity, and Molecular Docking of New Furan-2-one and Pyrazole heterocycles Based on 5,6,7,8-Tetrahydronaphthalene

Nehal A. Hamdy[a], Hanem M. Awad [b], Mohammad M.Tarek [c], Hanan A. Mohamed [a]*
[a] *Applied Organic Chemistry Department, Chemical Industries Research Institute, National Research Center, Dokki, Giza, 12622 Egypt;*
[b] *Department of Tanning Materials and Leather Technology, Chemical Industries Research Institute, National Research Centre, Dokki, 12622 Cairo, Egypt;*
[c] *Bioinformatics Department, Armed Forces College of Medicine (AFCM), Cairo, Egypt*

Abstract

Novel furan-2-one and pyrazole heterocycles incorporating 5,6,7,8-tetrahydronaphthalene moiety **4**, **8**, **10a-c**, **12a-c** and **13** were prepared starting from 2-acetyl tetralin via reaction with diethyl oxalate followed by cyclization using hydroxylamine hydrochloride, and hydrazine hydrate. Further treatment of carbohydrazide **8** with isatin derivatives **9a-c** and hydrazonoyl halides **11a-c** afforded *N*'-(5-subs.-2-oxoindolin-3-ylidene)-3-(5,6,7,8-tetrahydronaphthalen-2-yl)-1*H*-pyrazole-5-carbohydrazides **10a-c** and *N'*-aryl-2-(2-(3-(5,6,7,8-tetrahydronaphthalen-2-yl)-1*H*-pyrazole-5-carbonyl)hydrazono)propanehydrazonoyl chlorides **12a-c**. The novel compounds were examined in vitro for their anti-tumor activities against HepG-2 and MCF-7 human carcinoma cell lines using MTT assay. Most compounds showed good to moderate activities against HepG-2 carcinoma cells and HepG-2 cells.

Keywords: 2-Acetyl tetralin, Furan-2-ones, Pyrazoles, Anti-tumor activity.

1. Introduction

The methyl ketone, 2-acetyl tetralin, or 1-(5,6,7,8-tetrahydronaphthalen-2-yl)ethanone, is considered important raw material for the synthesis of biologically active compounds. Claisen condensation of methyl ketones with oxalic acid esters in the presence of strong base gave 2,4-dioxoesters which are valuable multi-purpose intermediates in organic synthesis [1]. 2,4-Dioxoesters are used in the synthesis of pyrazole-3(5)-ethyl esters [2] which are known to be important precursors in the preparation of herbicides, agrochemicals, microbicide [3] protectants and plant growth regulators [4]. Also, synthesis of 3-furanone ring system which is the key skeletal element of many natural product antitumor agents [5] In the view of the previous facts, we synthesized new heterocycles based on 5,6,7,8-tetrahydronaphthalene compounds as part of our continuing interest in the area of heterocycles with potential applications [6-13].

2. Experimental:

2.1. General

All melting points were taken on Electrothermal IA 9000 series digital melting point apparatus and were uncorrected. The IR spectra (KBr) were recorded on a Shimadzu CVT-04 spectrophotometer. The NMR spectra were measured with a JEOL E.C.A-500 MHz spectrometer using tetramethylsilane (TMS) as internal standard in DMSO-d6. Chemical shift (δ) values are given in parts per million. The mass spectra were determined using a Varian MAT CH-5 spectrometer (70 eV).

*Corresponding author e-mail: hananmoh257@gmail.com & hananm_2004@yahoo.com
Received: 3 May 2022; Revised 9 May 2022; Accepted 15 May 2022
DOI: 10.21608/EJCHEM.2022.136816.6032

2.1.1. Ethyl2,4-dioxo-4-(5,6,7,8-tetrahydronaphthalen-2-yl)butanoate (2)

A mixture of 2-acetyl tetralin **1** (1 mmol, 1.74 g) and diethyl oxalate (2 mmol, 2.92 g) in 25 cm^3 sodium ethoxide solution (0.005 g Na, 25 cm^3 ethanol) was refluxed for 1h., and then cooled. The solution was poured onto ice-water and neutralized with dilute hydrochloric acid (5%), extracted from ethyl acetate (50 ml * 3time) and evaporate the excess of ethyl acetate using the rotating evaporator to give 2 as oily compound.

Yield 90%. IR (KBr) $\nu_{max/cm}^{-1}$ 1660-1717 (C=O); ^{1}H NMR (DMSO-d6) δ 1.73 (m, 4H, 2 CH_2, tetrahydronaphthalene), 1.34 (t, 3H, J = 7.41Hz, CH_3), 2.74 (m, 4H, 2 CH_2, tetrahydronaphthalene), 4.24 (q, 2H, J = 7.41Hz, CH_2), 4.77 (s, 2H, CH_2), 7.05-7.54 (m, 2H, Ar-H), 7.62 (s, 1H, Ar-H). MS m/z (%): 274 (M^+, 100). Anal. Calcd for $C_{16}H_{18}O_4$ (274.31): C, 70.06; H, 6.61%. Found: C, 70.33; H, 6.94.

2.1.2. 3-(Hydroxyimino)-5-(5,6,7,8-tetrahydronaphthalen-2-yl)furan-2(3*H*)-one (4)

A mixture of compound **2** (2 mmol, 0.55 g) in ethanol (20 cm^3) and water (5 cm^3), hydroxylamine.HCl (0.14 g, 2 mmol) and potassium carbonate (0.27 g, 2 mmol) was refluxed for 6 h, then left to stand at room temperature. The product obtained was filtered off and dried.

Yield 55%; Mp 94-5°C. IR (KBr) $\nu_{max/cm}^{-1}$ 1652-1694 (C=O), 3280 (OH); ^{1}H NMR (DMSO-d6) δ 1.71 (m, 4H, 2 CH_2, tetrahydronaphthalene), 2.74 (m, 4H, 2 CH_2 , tetrahydronaphthalene), 7.03-7.36 (m, 4H, Ar-H + furanone-H), 10.96 (s, 1H, OH; exchangable). ^{13}C NMR (DMSO-d_6) δ 11.41, 22.60, 22.63, 28.93, 28.80, 121.56, 122.59, 126.02, 128.76, 134.16, 136.35, 137.13, 152.76. MS m/z (%): 243 (M+, 100). Anal. Calcd for $C_{14}H_{13}NO_3$ (243.26): C, 69.12; H, 5.39; N, 5.76%. Found: C, 69.41; H, 5.79; N, 5.70.

2.1.3. 3-(5,6,7,8-Tetrahydronaphthalen-2-yl)-1*H*-pyrazole-5-carbohydrazide (8)

Hydrazine hydrate (20 mmol, 1.0 g) was given to ethyl 2,4-dioxo-4-(5,6,7,8-tetrahydronaphthalen-2-yl) butanoate **2** (10 mmol, 2.74 g) in absolute ethanol (40 mL). The reaction mixture was boiled under reflux for 4 h and was then cooled, the formed solid was filtered off and recrystallized from dilute ethanol.

Yield 70%; Mp 300 °C. IR (KBr) $\nu_{max/cm}^{-1}$ 1604 (C=O), 3380-3150 (NH, NH_2); ^{1}H NMR (DMSO-d6) 1.72 (m, 4H, 2 CH_2, tetrahydronaphthalene), 2.73 (m, 4H, 2 CH_2, tetrahydronaphthalene), 4.47 (s, 2H, NH_2), 7.12-7.36 (m, 4H, Ar-H + pyrazole-H), 9.88 (s, 1H, NH; exchangeable), 11.45(s, 1H, NH; exchangeable). MS m/z (%): 256 (M+, 34), 200(100). Anal. Calcd for $C_{14}H_{16}N_4O$ (256.30): C, 65.61; H, 6.29; N, 21.86%. Found: C, 65.83; H, 6.60; N, 21.97.

2.1.4. N'-(5-Subs.-2-oxoindolin-3-ylidene)-3-(5,6,7,8-tetrahydronaphthalen-2-yl)-1*H*-pyrazole-5-carbohydrazides (10a-c)

A mixture of **8** (0.26 g, 1 mmol) and appropriate isatin derivatives **9a-c** (1 mmol) in absolute ethanol (30 mL) containing glacial acetic acid (1.0 ml) was heated under reflux for 6 h. The reaction mixture was cooled, and the formed colored solid was filtered off and dried.

2.1.4.1. *N*'-(2-Oxoindolin-3-ylidene)-3-(5,6,7,8-tetrahydronaphthalen-2-yl)-1*H*-pyrazole-5-carbohydrazide (10a)

Yield 76%; Mp 300 °C. IR (KBr) $\nu_{max/cm}^{-1}$ 1604 (C=O), 3310-3210 (NH); ^{1}H NMR (DMSO-d6) δ 1.71 (m, 4H, 2 CH_2, tetrahydronaphthalene), 2.74 (m, 4H, 2 CH_2, tetrahydronaphthalene), 6.95-7.95 (m, 8H, Ar-H + pyrazole-H), 11.42 (s, 1H, NH; exchangeable), 11.93 (s, 1H, NH; exchangeable), 14.16 (s, 1H, NH; exchangeable). MS m/z (%): 385 (M+, 18), 200(100). Anal. Calcd for $C_{22}H_{19}N_5O_2$ (385.42): C, 68.56; H, 4.97; N, 18.17 %. Found: C, 68.79; H, 5.14; N, 18.31.

2.1.4.2. *N*'-(5-Chloro-2-oxoindolin-3-ylidene)-3-(5,6,7,8-tetrahydronaphthalen-2-yl)-1*H*-pyrazole-5-carbohydrazide (10b)

Yield 74%; Mp 300 °C. IR (KBr) $\nu_{max/cm}^{-1}$ 1598 (C=O), 3310-3210 (NH); 1H NMR (DMSO-d6) δ 1.73 (m, 4H, 2 CH_2, tetrahydronaphthalene), 2.73 (m, 4H, 2 CH_2, tetrahydronaphthalene), 6.97-7.95 (m, 7H, Ar-H + pyrazole-H), 11.52 (s, 1H, NH; exchangeable), 12.02 (s, 1H, NH; exchangeable), 14.12 (s, 1H, NH; exchangeable). MS m/z (%): 420 (M^+, 20), 200(100). Anal. Calcd for $C_{22}H_{18}ClN_5O_2$ (419.86): C, 62.93; H, 4.32; N, 16.68%. Found: C, 63.12; H, 4.51; N, 16.84.

2.1.4.3. *N*'-(5-Bromo-2-oxoindolin-3-ylidene)-3-(5,6,7,8-tetrahydronaphthalen-2-yl)-1*H*-pyrazole-5-carbohydrazide (10c)

Yield 78%; Mp 300 °C. IR (KBr) $\nu_{max/cm}^{-1}$ 1608 (C=O), 3310-3190 (NH); ^{1}H NMR (DMSO-d6) δ 1.73 (m, 4H, 2 CH2, tetrahydronaphthalene), 2.73 (m, 4H, 2 CH_2, tetrahydronaphthalene), 6.89-7.68 (m, 7H, Ar-H + pyrazole-H), 9.89 (s, 1H, NH; exchangeable), 11.37 (s, 1H, NH; exchangeable), 13.95 (s, 1H, NH; exchangeable). MS m/z (%): 466 (18), 465 (19), 464 (M^+, 20), 200 (100). Anal. Calcd for $C_{22}H_{18}BrN_5O_2$ (464.31): C, 56.91; H, 3.91; N, 15.08%. Found: C, 57.33; H, 4.09; N, 15.48.

2.1.5. *N*'-Aryl-2-(2-(3-(5,6,7,8-tetrahydronaphthalen-2-yl)-1H-pyrazole-5-carbonyl)hydrazono)propanehydrazonoyl chlorides (12a-c)

A mixture of carbohydrazide **5** (10 mmol, 2.56 g) and 2-oxo-*N*-arylpropanehydrazonoyl chloride 11a-c (10 mmol) in absolute ethanol (30 mL) was refluxed for 5 h. Then left to cool, the formed solid was filtered off, washed with ethanol, and recrystallized from EtOH/DMF.

2.1.5.1. (1*Z*,2*E*)-*N*'-phenyl-2-(2-(3-(5,6,7,8-tetrahydronaphthalen-2-yl)-1*H*-pyrazole-5-carbonyl)hydrazono)propanehydrazonoyl chloride (12a)

Yield 72%; Mp 270-1 °C. IR (KBr) $\nu_{max/cm}^{-1}$ 1602 (C=O), 3310-3190 (NH); ^{1}H NMR (DMSO-d_6) δ 1.72 (m, 4H, 2 CH2, tetrahydronaphthalene), 2.34 (s, 3H, CH_3), 2.71 (m, 4H, 2 CH_2, tetrahydronaphthalene), 6.71-7.37 (m, 9H, Ar-H + pyrazole-H), 10.24 (s, 1H, NH; exchangeable), 10.76 (s, 1H, NH; exchangeable), 14.12 (s, 1H, NH; exchangeable). Anal. Calcd for $C_{23}H_{23}ClN_6O$ (434.92): C, 63.52; H, 5.33; N, 19.32%. Found: C, 63.74; H, 5.48; N, 19.52.

2.1.5.2. (1*Z*,2*E*)-*N*'-(4-chlorophenyl)-2-(2-(3-(5,6,7,8-tetrahydronaphthalen-2-yl)-1*H*-pyrazole-5-carbonyl)hydrazono)propanehydrazonoyl chloride (12b)

Yield 76%; Mp 290-2 °C. IR (KBr) $\nu_{max/cm}^{-1}$ 1603 (C=O), 3280-3180 (NH); 1H NMR (DMSO-d6) δ 1.71 (m, 4H, 2 CH2, tetrahydronaphthalene), 2.32 (s, 3H, CH3), 2.72 (m, 4H, 2 CH_2, tetrahydronaphthalene), 7.28-7.36 (m, 8H, Ar-H + pyrazole-H), 10.09 (s, 1H, NH; exchangeable), 11.45 (s, 1H, NH; exchangeable), 13.85 (s, 1H, NH; exchangeable). Anal. Calcd for $C_{23}H_{22}Cl_2N_6O$ (469.37): C, 58.86; H, 4.72; N, 17.91%. Found: C, 58.95; H, 4.88; N, 18.09.

2.1.5.3. (1*Z*,2*E*)-*N*'-(4-Bromophenyl)-2-(2-(3-(5,6,7,8-tetrahydronaphthalen-2-yl)-1*H*-pyrazole-5-carbonyl)hydrazono)propanehydrazonoyl chloride (12c)

Yield 75%; Mp 284-5 °C. IR (KBr) $\nu_{max/cm}^{-1}$ 1601 (C=O), 3280-3180 (NH); ^{1}H NMR (DMSO-d6) δ 1.72 (m, 4H, 2 CH_2, tetrahydronaphthalene), 2.33 (s, 3H, CH_3), 2.74 (m, 4H, 2 CH_2, tetrahydronaphthalene), 7.23-7.42 (m, 8H, Ar-H + pyrazole-H), 10.36 (s, 1H, NH; exchangeable), 10.76 (s, 1H, NH; exchangeable), 13.55 (s, 1H, NH; exchangeable). Anal. Calcd for $C_{23}H_{22}BrClN_6O$ (513.82): C, 53.76; H, 4.32; N, 16.36%. Found: C, 53.91; H, 4.56; N, 16.71.

2.6. *N*'-(1-(2-Phenylhydrazono)-1-(phenylsulfonyl)propan-2-ylidene)-3-(5,6,7,8-tetrahydronaphthalen-2-yl)-1*H*-pyrazole-5-carbohydrazide (13).

To a solution of the propanehydrazonoyl chloride **12a** (1 mmol, 0.44 g) in absolute ethanol (30 mL), sodium benzenesulphinate dihydrate (0.4 g, 2 mmol) was added. The mixture was refluxed for 12 h, then left to cool. The reaction mixture was poured into cold water and the solid product filtered off, washed with water, dried, and finally recrystallized from EtOH/DMF to afford the corresponding sulphone **13**.

Yield 62%; Mp 178-9°C. IR (KBr) $\nu_{max/cm}^{-1}$ 1596 (C=O), 3280-3180 (NH); 1H NMR (DMSO-d6) δ 1.72 (m, 4H, 2 CH_2, tetrahydronaphthalene), 2.31 (s, 3H, CH_3), 2.74 (m, 4H, 2 CH_2, tetrahydronaphthalene), 6.86-7.38 (m, 14H, Ar-H + pyrazole-H), 9.94 (s, 1H, NH; exchangeable), 11.45 (s, 1H, NH; exchangeable), 13.81 (s, 1H, NH; exchangeable). MS m/z (%): 542(6), 541(20), 540 (M^+, 42), 315(100). Anal. Calcd for $C_{29}H_{28}N_6O_3S$ (540.64): C, 64.43; H, 5.22; N, 15.54%. Found: C, 64.63; H, 5.57; N, 15.74.

2.2. In-vitro cell culture conditions

The HepG-2 (human liver carcinoma) and MCF-7 (human breast adenocarcinoma) cell lines were purchased from the American Type Culture Collection (ATCC) and maintained in DMEM medium which was supplemented with 10% heat-inactivated FBS (fetal bovine serum), 100U/ml penicillin and 100U/ml streptomycin. The cells were grown at 37°C in a humidified atmosphere of 5% CO_2 [9].

2.2.1. MTT cytotoxicity assay

The antitumor activity on HepG-2 and MCF-7 human cancer cell lines was estimated using the 3-[4,5-dimethyl-2-thiazolyl)-2,5-diphenyl-2H-tetrazolium bromide (MTT) assay, which is based on the cleavage of the tetrazolium salt by mitochondrial dehydrogenases in viable cells [14]. Cells were dispensed in a 96 well sterile microplate (1 x 10^4 cells/well), and incubated at 37^{o}C with series of different concentrations, in DMSO, of each tested compound or Doxorubicin® (positive control) for 48 h in a serum free medium prior to the MTT assay. After incubation, media were carefully removed, 40 µL of MTT (2.5 mg/mL) were added to each well and then incubated for an additional 4 h. The purple formazan dye crystals were solubilized by the addition of 200 µL of DMSO. The absorbance was measured at 570 nm using a SpectraMax® Paradigm® Multi-Mode microplate reader. The relative cell viability was expressed as the mean percentage of viable cells compared to the untreated control cells.

2.3. Computational Methods

2.3.1. Target fishing

Target fishing for the synthesized compounds was performed through determination of potential target families for each compound using Polypharmacology browser [15] tool as a multi-fingerprint-based prediction method that could compute possible analogs of shared fingerprints through searching 4613 chemical groups of curated molecules in ChEMBL database. The Target fishing procedure was performed with the aim of providing targets that could explain the experimental anticancer activity of the synthesized compounds.

2.3.2. Target Fishing Results

Polypharmacology browser tool predicted MCF-7 and HepG2 cell lines to include potential targets for the nine compounds, and further mining of screening results revealed possible targeting of tyrosine kinases including hepatocyte growth factor receptor (c-Met) which was predicted as fishing hit for the nine compounds and epidermal growth factor receptor (EGFR). Poly (ADP-ribose) polymerase 1 (PARP1), a potential target for BRCA1 positive breast cancer that was found to be a hit target for compounds (8, 10a and 12a). Thus, we have selected c-Met as a potential target of variety of cancers including hepatocellular carcinoma [16] and PARP1 as potential target for breast cancer drug therapy [17] to further investigate through computational studies the binding effectiveness in comparison to approved drugs for both targets. Other interesting targets were found including cellular tumor antigen TP53 in which targeting could further explain the anticancer activity of the newly synthesized compounds (Supplementary File-1).

2.3.3. Preparation of Ligands and Target Structure

The 2D representation of the nine compounds was prepared in MOL format and then was subjected to energy minimization using Chem3D Ultra through MM2 force field. Furthermore, the nine compounds were consequently subjected to MOPAC module semi empirical AMI method with 0.1 root mean square (RMS) gradient. The prepared structures were then converted to PDBQT format before docking through MGL tools.

The c-MET structure was retrieved from (PDB: 2WGJ) [18] and the PARP1 structure from (PDB: 5DS3) [19] both structures were optimized by removing water and solvent atoms. The refined structures were further prepared for docking by adding polar hydrogens and merging non-polar hydrogens using MGL tools. Grid box was prepared and centered on the active site of olaparib on PARP-1 and crizotinib on c-MET crystal structures.

2.3.4. Docking simulations using AutoDock vina

Docking simulations was designed on defining flexible binding site against possible ligands. AutoDock Tools were used to select flexible residues which were reported to have significant contribution to the interaction between olaparib and PARP-1 as well as crizotinib and c-MET. AutoDock vina was then used to run flexible docking simulations for each compound as well as both ligands [20, 21]. The default scoring function was used. Post-docking ligand interaction 2D diagrams were studied using Protein Ligand Interaction profiler (PLIP) [22] and while docking poses were visualized using PyMOL v2.3.2 [23] and LigPlot+[26]. Default scoring function was used for docking. Binding modes of the docked complexes were obtained and the amino acid residues present at a distance of 5Å were considered as the binding partners of the ligands. The interaction diagrams representing the docked complexes have

been generated using PyMOL v 2.3.2. Docking simulations were run using AutoDock 4.2.3 and AutoDock vina 1.1.2 with MGL tools 1.5.6.

4.Results and Discussion

Condensation of 2-acetyl tetralin **1** with diethyl oxalate in the presence of sodium ethoxide followed by acidification of the resulting solution with dilute acetic acid give excellent yields of ethyl 2,4-dioxo-4-(5,6,7,8-tetrahydronaphthalen-2-yl)butanoate **2** which used a precursor for the synthesis of target heterocycles (Scheme 1). 3-(Hydroxyimino)-5-(5,6,7,8-tetrahydronaphthalen-2-yl)furan-2(3*H*)-one **4** was prepared, in 55 % yield, through the reaction of **2** and hydroxylamine hydrochloride in the presence of molar ratio from potassium carbonate ethanol at reflux condition. There was no evidence for the formation of the expected product, (ethyl 5-(5,6,7,8-tetrahydronaphthalen-2-yl)isoxazole-3-carboxylate **5** (Scheme 1).

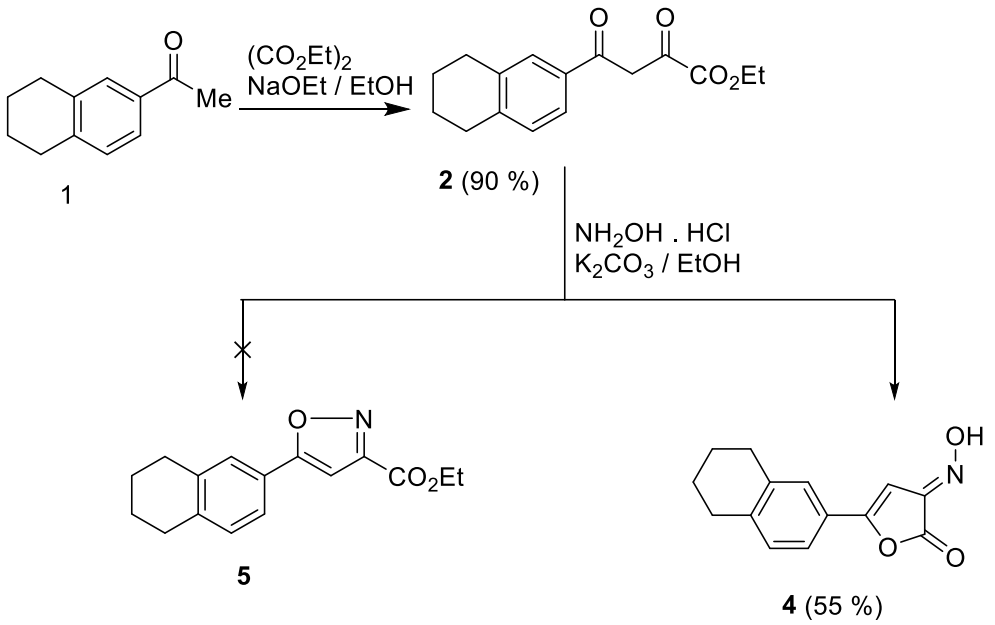

Scheme 1. synthesis of furan-2-one 4

The proposed mechanism for the formation of product 4 illustrated in Scheme 2. Reaction of **2** with hydroxylamine hydrochloride gave ethyl 2-(hydroxyimino)-4-oxo-4-(5,6,7,8-tetrahydronaphthalen-2-yl)butanoate **6** as an intermediate. The reaction preceded via an elimination of ethanol molecule from the enol intermediate **7** to furnish the target furan-2-one **4** (Scheme 2).

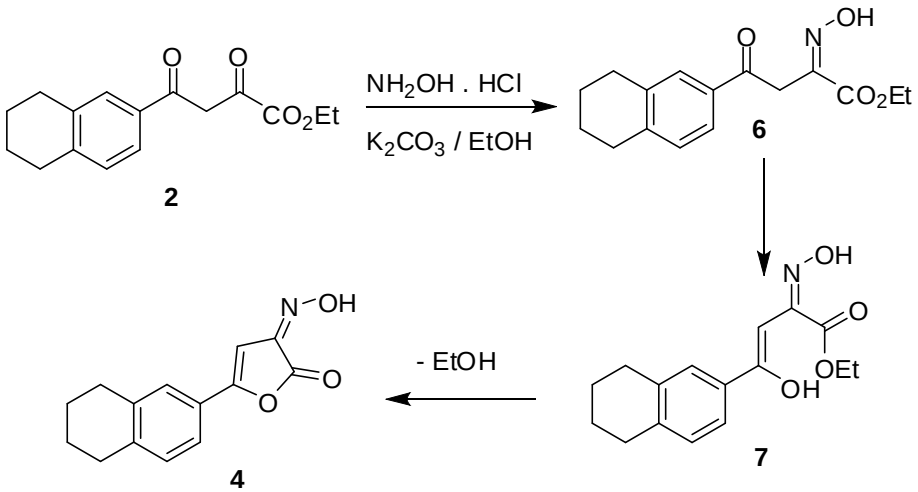

Scheme 2. Proposed mechanism for the synthesis of 4.

The structure of the compound **4** was confirmed by spectral and analytical data. For example, the IR spectrum of compound **4** showed peaks that resonate at ν 1652-1694 and 3280 cm^{-1} corresponding to C=Ostr., and O-Hstr., respectively. In its ^1H NMR spectrum shows the one oxime proton at 10.96 ppm.

Refluxing ethyl 2,4-dioxobutanoate **2** with excess hydrazine hydrate in anhydrous ethanol afforded 3-(5,6,7,8-tetrahydronaphthalen-2-yl)-1*H*-pyrazole-5-carbohydrazide 8 in about 70% yield (Scheme 3).

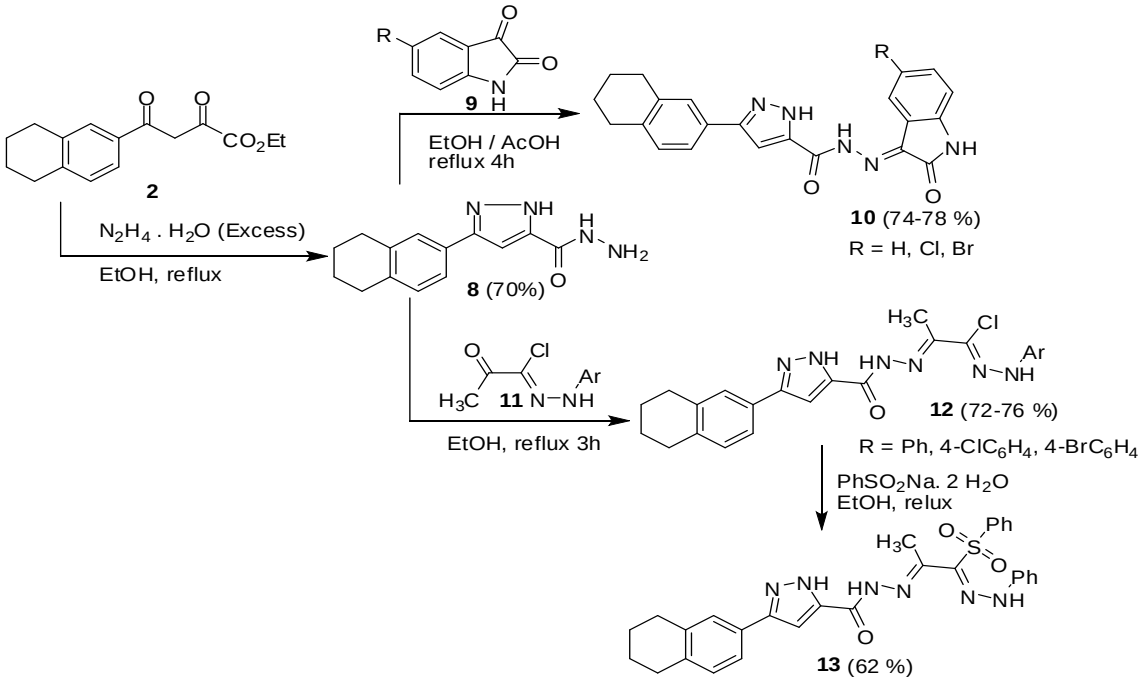

Scheme 3: Synthesis of pyrazoles 8, 10a-c, 12a-c and 13

Reaction of pyrazole-5-carbohydrazide **8** with three isatin derivatives **9a-c** in refluxing ethanol and in the presence of catalytic amount of glacial acetic acid, as dehydrating agent, afforded *N'*-(5-subs.-2-oxoindolin-3-ylidene)-3-(5,6,7,8-tetrahydronaphthalen-2-yl)-1*H*-pyrazole-5-carbohydrazides **10a-c** in 74-78 % yields. *N*'-aryl-2-(2-(3-(5,6,7,8-tetrahydronaphthalen-2-yl)-1*H*-pyrazole-5-carbonyl)hydrazono)propanehydrazonoyl chlorides **12a-c** were prepared, in 72-76 % yields, by treatment of pyrazole-5-carbohydrazide **8** with hydrazonoyl chlorides **9a-c** in refluxing dry ethanol for 3h. Further treatment of **12a** with sodium benzenesulfinate dihydrate in aqueous ethanol (70 %) afforded N'-(1-(2-phenylhydrazono)-1-(phenylsulfonyl)propan-2-ylidene)-3-(5,6,7,8-tetrahydronaphthalen-2-yl)-1*H*-pyrazole-5-carbohydrazide **13** in about 62 % yield (Scheme 3).

The ^1H NMR spectra of hydrazones **12a-c** and **13** show a singlet at about 2.30 ppm due to methyl group. Also, their IR spectra exhibit a peak in the range 3310-3210 cm^{-1} corresponding to the NH groups.

Anti-proliferative activity

Selected compounds were examined in vitro for their anti-tumor activities against HepG-2 and MCF-7 human carcinoma cell lines using MTT assay.

The obtained results showed that all compounds showed dose-dependent anticancer activities on both cancer types.

From the data presented in Table 1, it is obvious that, all compounds have good cytotoxicity effects on both cancer types. The order of the decreasing activity on the human liver cancer type (HepG2) is as follow: **4** > **12b** > **10a** > **12c** > **10c** > **8** > doxorubicin > **12a** > **10b** >**13**. The rest of the compounds showed moderate activities against HepG-2 cells. However, the order of the decreasing activity on the human breast cancer type (MCF-7) is as follow: **4** > **10a** > **12b** > **12c** > **8** > **12a** > **10c** > doxorubicin >**10b** > **13**.

Table 1: The Anti-proliferative IC_{50} values of the nine compounds using MTT assay on two cancer types.

compounds	IC_{50} (μM) ± SD	
	HepG-2	MCF-7
4	65.8 ± 3.2	56.3± 2.1
8	78.1 ± 3.8	64.1± 2.7
10a	76.1 ± 2.7	62.1± 3.9
10b	90.6 ± 4.1	67.4 ± 2.7
10c	76.9 ± 3.6	64.6± 2.3
12a	83.5 ± 2.5	64.1± 2.5
12b	75.8 ± 3.5	62.7± 3.7
12c	76.3 ± 2.5	63.7± 2.8
13	100.0 ± 3.9	74.1± 3.3
Doxorubicin	80.9± 2.1	65.5± 2.4

Hepatocyte growth factor receptor (c-Met) docking results

Docking simulations using Auto Dock vina revealed significant interactions between the nine compounds and c-Met with apparent compatibility to the crizotinib binding pocket. The docking simulations generated binding affinities through the default scoring function of vine as visualized in Figure 1 through PyMOL visualization of best docking poses for each docking run. Table 2 further represents the generated binding energies of the nine compounds as well as crizotinib. Additionally, it shows the residues involved in ligand interaction surrounding the binding pocket at 4 Å which were generated using PLIP tool in Figure 2. The binding pocket of crizotinib against c-Met was further analyzed to reveal the characters of the necessary interactions for selective inhibition of human c-Met. Crizotinib interacts with its binding pocket through extensive hydrophobic interactions with residues Val1092, Leu1157 and Tyr1230 and hydrogen bonding with Pro1158 and Met1160 along with aromatic π-π interaction through halogenated phenyl group with Tyr1230 (Figure 2).

Regarding the computed affinities, compounds **10a**, **10c**, **12b** and **13** exhibited the most stable binding with the lowest ΔGb compared to the computed binding energy of the approved drug crizotinib. Moreover, compound **13** exhibited the most stable docking poses with -11.1 kcal/mol binding free energy. This stable interaction could be represented in Table 2 through the binding interactions including aromatic interactions through parallel π-stacking with Tyr1230 which turns to be crucial for binding affinity of crizotinib. Compound 13 also showed hydrogen bonding with Asn1167 and Asn1171 as well as hydrophobic interactions with Val1092, Leu1157, His1162, Asn1167, Phe1168, Arg1170, Asn1171, Ala1226 andTyr1230.

Another group of compounds showed stable binding as well including 10a, 10c and 12b with -10.5, -10.5 and -10.6 kcal/mol binding energy respectively. All nine compounds showed strong aromatic interaction (Figure 2) as they exhibited π-π interaction with Tyr1230 which is a typical character of crizotinib. Hydrophobic van der Waal's interactions represented an important contributor to the interaction among the nine compounds as well as crizotinib where residue Tyr896 was frequently involved in the hydrophobic binding pocket that surrounds the pyrazole ring in compounds **8**, **10b**, **10c**, **12a**, **12b**, **12c** and **13** which describes the role of non-polar interactions. Polar Interactions were also important for linking functional groups of the docked compounds into main residues in the predefined binding site. Furthermore, residue Asn1167 established apparent hydrogen bonding with all nine compounds as visualized in docking poses at Figure 1. These docking results are in agreement with the cytotoxic screening results of the nine compounds.

Poly (ADP-ribose) polymerase 1 (PARP1) docking results

Docking simulations using Auto Dock vina revealed significant interactions between the nine compounds and PARP1 with apparent compatibility to the olaparib binding pocket. The docking simulations generated binding affinities through the default scoring function of vina as visualized in Figure 3 through PyMOL visualization of best docking poses for each docking run. Table 2 further represents the generated binding energies of the nine compounds as well as Olaparib. Additionally, it

shows the residues involved in ligand interaction surrounding the binding pocket at 4 Å obtained from PLIP tool in Figure 4. The binding pocket of olaparib against PARP1 was further analyzed to reveal the characters of the necessary interactions for selective inhibition of human PARP1. Olaparib interacts with its binding pocket through extensive hydrophobic interactions with residues Tyr889 Tyr896 and Tyr07 and hydrogen bonding with Gly863, Arg878 and Tyr896 as well as π-π interaction with Tyr896 and Tyr907 which position the pyrimidine ring through the nicotinamide binding pocket (Figure 4).

Regarding the computed affinities, compounds **10a**, **10b**, **10c** and **13** exhibited the most stable binding with the lowest ΔGb compared to the computed binding energy of the approved drug olaparib. Moreover, compounds 10b and 10c exhibited the most stable docking poses with -12.4 kcal/mol binding free energy. This stable interaction could be represented in Table 2 through the binding interactions including aromatic interactions through parallel π-stacking with Tyr907. Both compounds also showed hydrogen bonding with His862, Ser964, Asn868, Gly876 and Arg878 as well as hydrophobic interactions with Tyr896, Ala898, Lys903 and Glu988.

Another group of compounds showed stable binding as well including 13 and 10a with -11.0 and -11.9 kcal/mol binding energy respectively. All nine compounds showed strong aromatic interaction (Figure 3) as they exhibited π-π interaction with Tyr907 which is a typical character of olaparib. Although compounds 4 and 12a noticeably showed the highest ΔGb, they still show strong interaction with the predefined nicotinamide binding pocket. Hydrophobic van der Waal's interaction was important contributor to the interaction among the nine compounds as well as olaparib where residues Val1092, Leu1157 were frequently involved in the hydrophobic binding pocket that surrounds the pyrazole ring in compounds **8**, **10b**, **10c**, **12a**, **12b** and **13** which describes the role of non-polar interactions. Polar Interactions were also linking functional groups of the docked ligands into main residues in the predefined binding site. Furthermore, residue Arg878 established apparent hydrogen bonding with the highly stable docked ligands **10b**, **10c**, **12a**, **12b**, **12c** and **13** as visualized in docking poses at Figure 3.

Table 2: The approximate free energies of binding (ΔGb) of the nine compounds and the corresponding approved ligand **14** in the catalytic sites of both c-Met and PARP1 and neighboring residues at 4 Å computed by Autodock vina.

Compound Code	c-Met-Affinity	Interacting residues with c-Met	PARP1-Affinity	Interacting residues with PARP-1
4	-9.0	Hydrophobic (Val1092, Asp1222, Ala1226, Tyr1230), HBonds (Asn1167), P(Tyr1230)	-9.9	Hydrophobic (Ala898, Lys903, Tyr907), HBonds (Ser864, Arg865, Asn868), P(Tyr907)
8	-10.0	Hydrophobic (Val1092,Leu1157,Ala1226,Tyr1230), HBonds (Ile1084, Asp1164, Arg1166, Asn1167, Asp1231, P(Tyr1230))	-10.6	Hydrophobic (Tyr896, Ala898, Lys903, Glu988), HBonds (His862, Asn868), P(Tyr907)
10a	-10.5	Hydrophobic (Arg1086, Val1092, Leu1140, Leu1157, Ala1221, Ala1226), HBonds (Asp1164, Asn1167, Tyr1230), P(Tyr1230)	-11.9	Hydrophobic (ILE872), HBonds (His862, Gly863, Lys903, Tyr907, Glu988), P(Tyr907), Aromatic (His862)
10b	-10.4	Hydrophobic (Val1092, Leu1157, Ala1221, Ala1126, Tyr1230), HBonds (Asp1164, Asn1167), P(Tyr1230)	-12.4	Hydrophobic (Tyr896, Ala898, Lys903, Glu988), HBonds (His862, Ser964, Asn868, Gly876, Arg878),

				P(Tyr907)
10c	-10.5	Hydrophobic (Val1092, Leu1157, Ala1221, Ala1126, Tyr1230), HBonds (Asp1164, Asn1167), P(Tyr1230)	-12.4	Hydrophobic (Tyr896, Ala898, Lys903, Glu988), HBonds (His862, Ser964, Asn868, Gly876, Arg878), P(Tyr907)
12a	-10.3	Hydrophobic (Val1092, Leu1157, Asn1167, Arg1170, Asn1171, Ala1226), HBonds (Asn1167, Asn1171), P(Tyr1230)	-10.5	Hydrophobic (Arg878, Tyr896, Glu988), HBonds (Ser864, Asn868, Arg878), P(Tyr907)
12b	-10.6	Hydrophobic (Val1092,Leu1157, Asn1167, Arg1170,Asn1171,Asp1222 Ala1226), HBonds (Asn1167,Asn1171), P(Tyr1230)	-10.7	Hydrophobic (Ile872, Tyr896, Glu988), HBonds (Ser864, Arg878), P(Tyr907)
12c	-10.4	Hydrophobic (Leu1157, Asn1167, Arg1170,Asn1171,Asp1222 Ala1226), HBonds (Asn1167,Asn1171), P(Tyr1230)	-10.7	Hydrophobic (Ile872, Tyr896, Glu988), HBonds (Ser864, Arg878), P(Tyr907)
13	-11.1	Hydrophobic (Val1092,Leu1157, His1162, Asn1167, Phe1168, Arg 1170, Asn1171, Ala1226, Tyr1230), HBonds (Asn1167,Asn1171), P(Tyr1230)	-11.0	Hydrophobic (Tyr896), HBonds (Arg878), P(Tyr907)
Approved Ligand (**14**)	-10.4 (Crizotinib)	Hydrophobic (Val1092, Leu1157, Tyr1230), HBonds (Pro1158, Met1160), P(Tyr1230), Halogen bond (Ile1084)	-10.8 (Opalarib)	Hydrophobic (Tyr889, Tyr896, Tyr907), HBond (Gly863, Arg878, Tyr896), P(Tyr896), P(Tyr907)

The geometrical orientation of the nine docked compounds preserved the allocation within the binding sites of crizotinib on c-Met and olaparib on PARP1 which could explain their competitive binding affinities compared to the corresponding approved ligand. Therefore, these compounds could be promising ligands for selective inhibition of c-Met and other tyrosine kinases as well as PARP1 which might explain the observed anticancer activity of these compounds in screening assay against HepG-2 and MCF-7 cell lines. Although the computational study provided promising docking results regarding selective inhibition of c-Met and PARP1, the topology of the defined binding sites should be considered for further molecular dynamics simulations and specific binding assays.

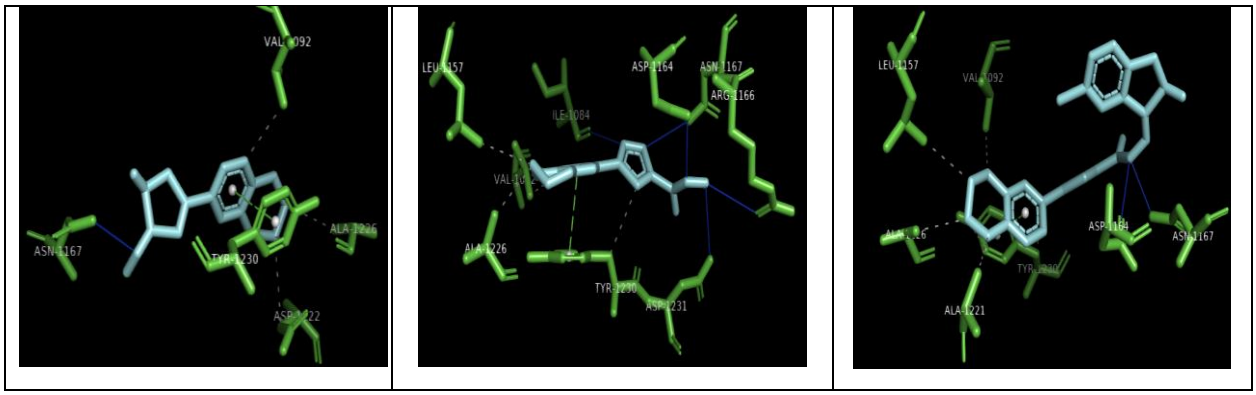

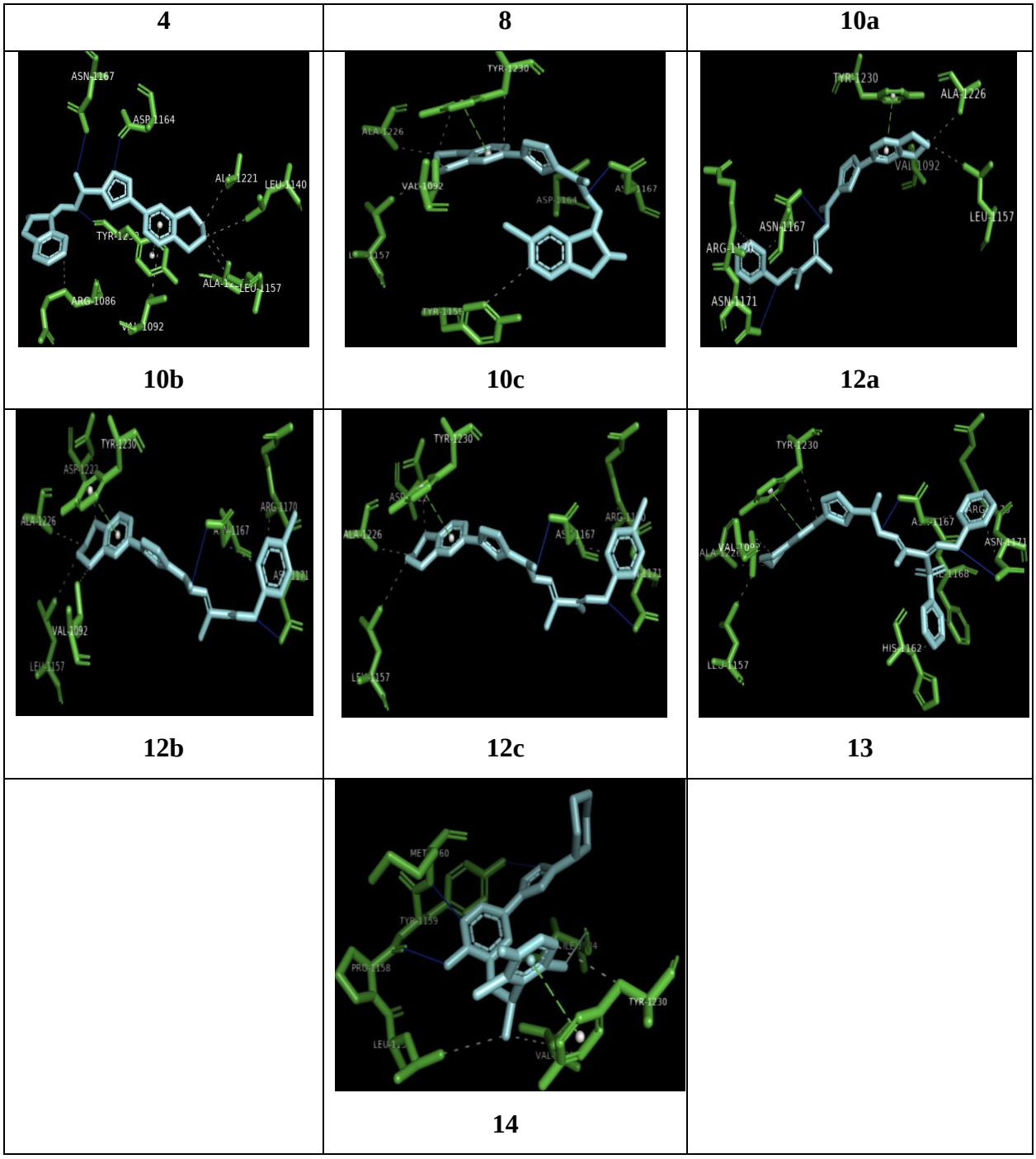

Figure 1: Visualized poses of the nine compounds and crizotinib (**14**) docked into c-Met represented using PyMOL. Ligands are colored in cyan while labeled binding sites in green, hydrogen blonds in blue lines, hydrophobic interactions in dashed grey lines and aromatic interactions in dashed green lines**.**

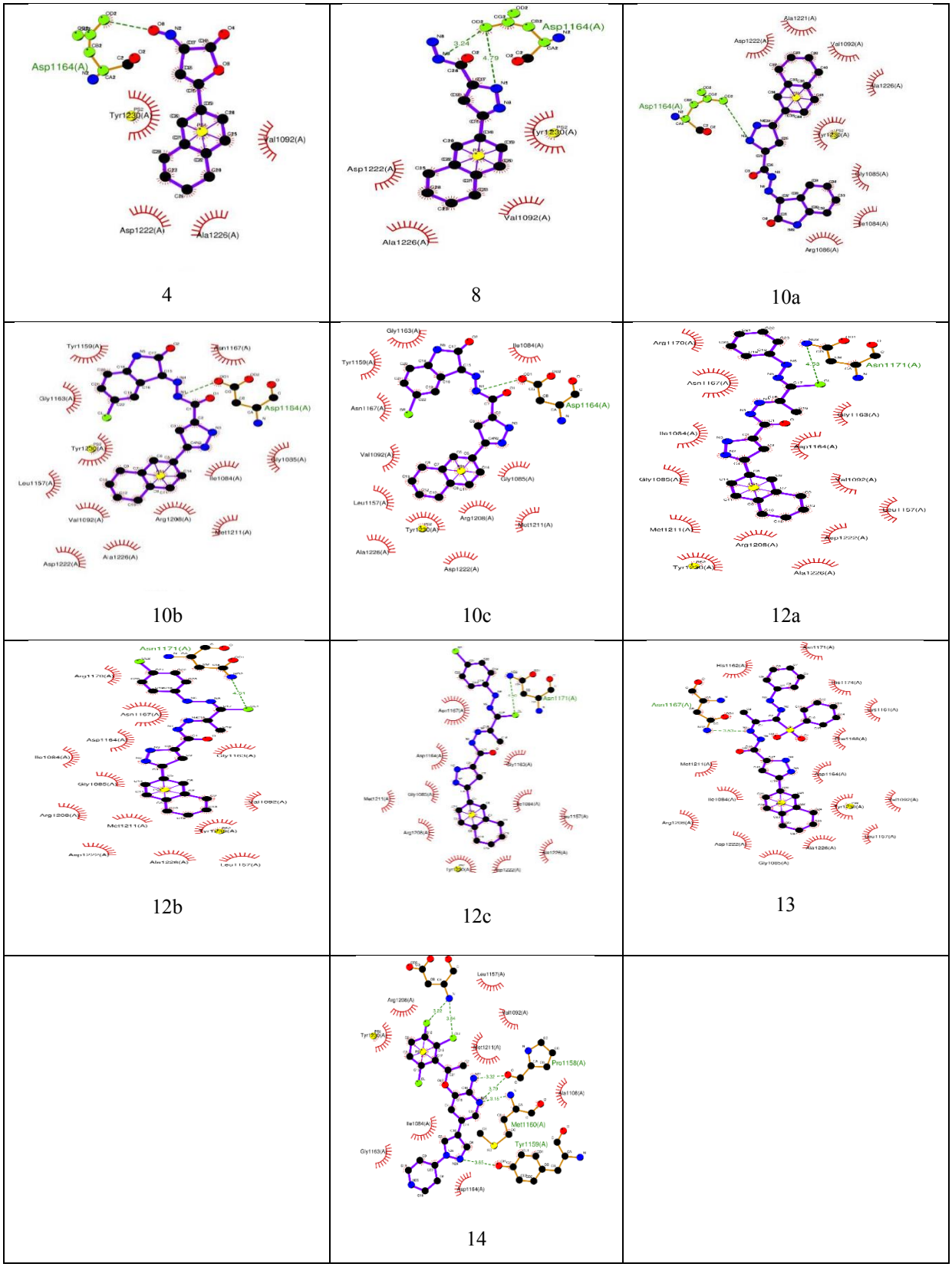

Figure 2: Representative 2D-Ligand interaction diagrams for the nine compounds and crizotinib (14) using LigPlot+.

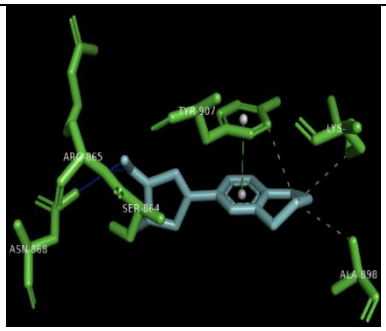

4

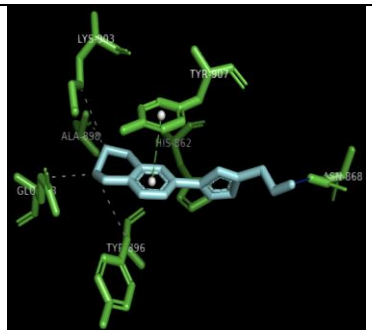

8

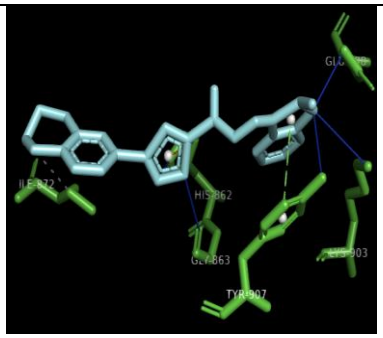

10a

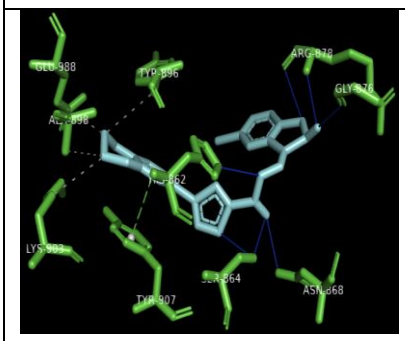

10b

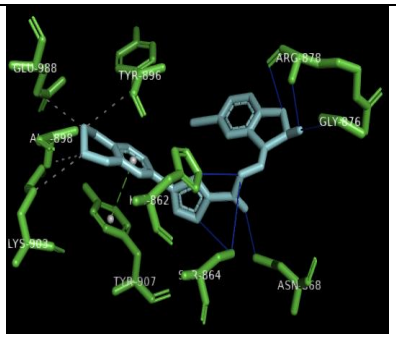

10c

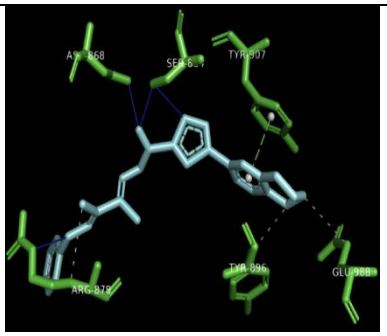

12a

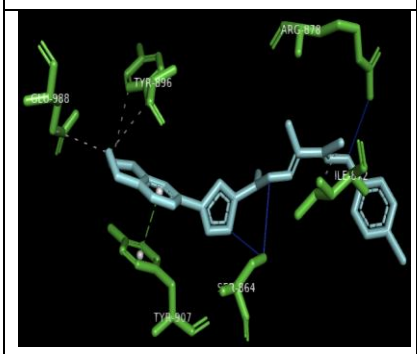

12b

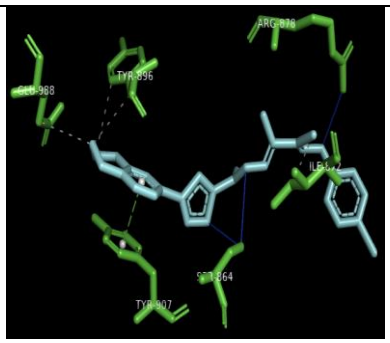

12c

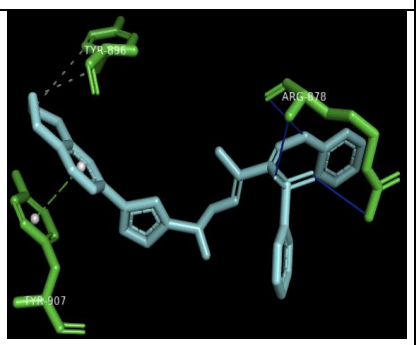

13

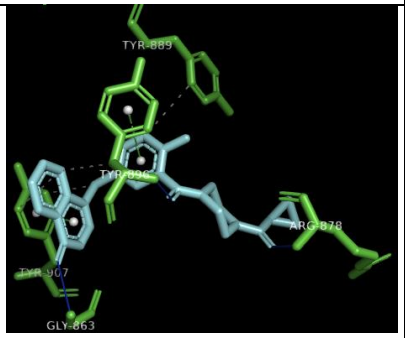

14

Figure 3: Visualized poses of the nine compounds and olaparib (**14**) docked into PARP1 represented using PyMOL. Ligands are colored in cyan while labeled binding sites in green, hydrogen blonds in blue lines, hydrophobic interactions in dashed grey lines and aromatic interactions in dashed green lines.

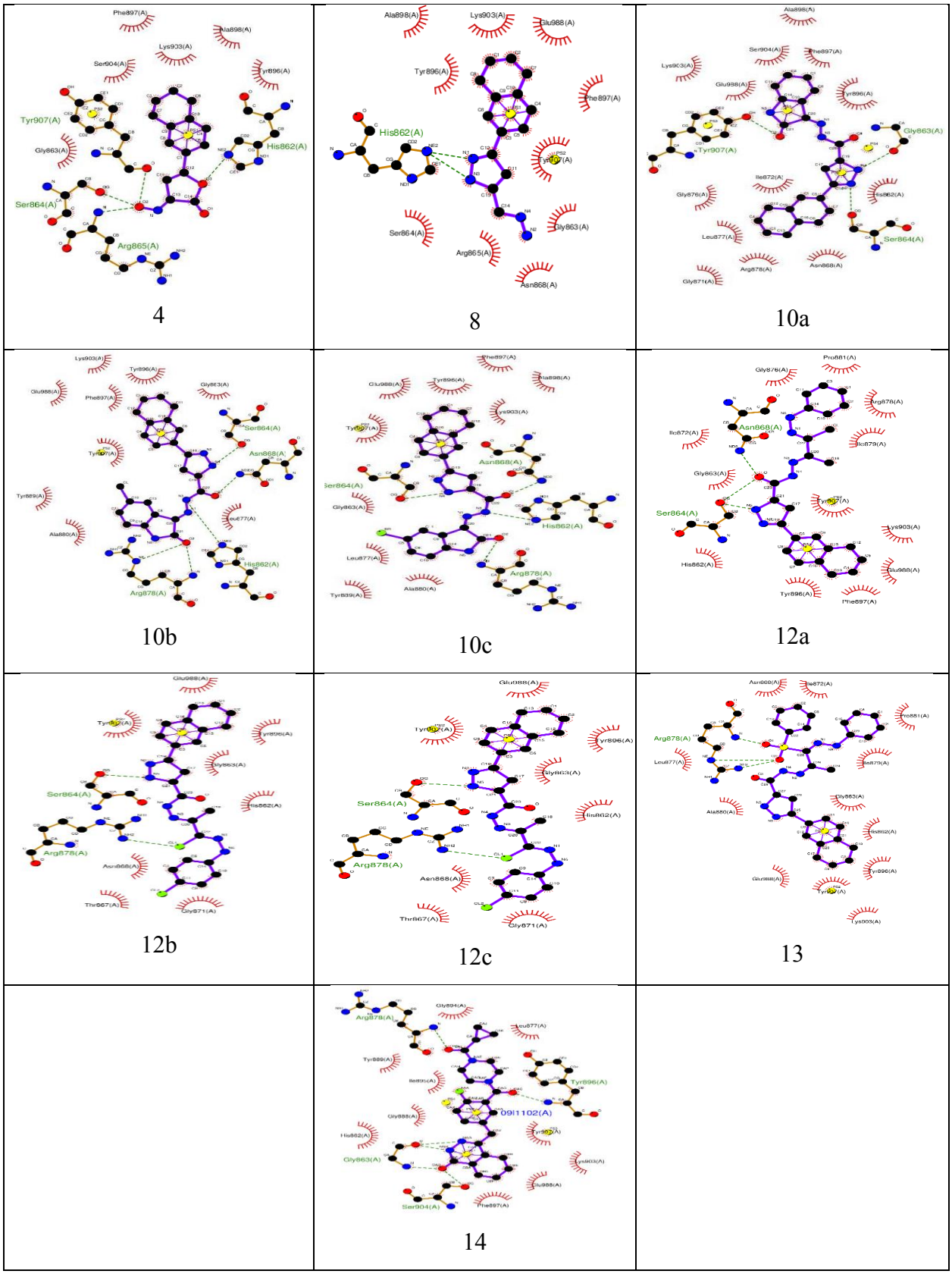

Figure 4: Representative 2D-Ligand interaction diagrams for the nine compounds and olaparib (**14**) against PARP1 using LigPlot+.

5. Conclusions

Novel 5,6,7,8-tetrahydronaphthalene bearing furan-2-one and pyrazole heterocycles were prepared according to the previously published methods. The new heterocycles were examined in vitro for their anti-tumor activities against HepG-2 and MCF-7 human carcinoma cell lines using MTT assay and the initial results showed good anticancer activities against both human liver (HepG-2) and human breast (MCF-7) carcinoma types. The anticancer screening results are in agreement with the docking results against hepatocyte growth factor receptor, as a potential target of variety of cancers including hepatocellular carcinoma, and PARP1, as potential targets for breast cancer drug therapy.

Conflicts of interest

"There are no conflicts to declare".

6. References

[1] Dawood K.M., Abdel-Gawad H., Mohamed H.A., Abdel-Wahab B.F. Utility of 2,4-dioxoesters in the synthesis of new heterocycles. *Heterocycles*, 2010, 81, 1-55.

[2] Khidre R.E., Abdel-Wahab B.F., Farahat A.A., Mohamed H.A. Synthetic routes to pyrazole-3(5)-carboxylates. *J. Heterocycl.Chem.,* 2016, 53, 13-31.

[3] Paporisch A., Rubin B. Isoxadifen safening mechanism in sweet corn genotypes with differential response to P450-metabolized herbicides. *Pestic Biochem. Physiol*., 2017, 138, 22-28.

[4] Kawase M., Koiwai H Synthesis of trifluoromethyl-substituted pyrazoles and 1,2,4-triazines by ring transformation of mesoionic 4-trifluoroacetyl-1,3-oxazolium-5-olates with phenylhydrazine. *Chem. Pharm. Bull*. (Tokyo)., 2008, 56, 433-8.

[5] Baraldi P. G., Barco A., Benetti S., Manfredini S., Pollini G. P., Simoni D. Ethyl 2,4-dioxoalkanoates as starting materials for a convenient route to 3(2H) furanones and 3(2H) furanimines. *Tetrahedron*, 1987, 43, 235-242.

[6] Hamza, E.K., Hamdy, N.A., Zarie, E.S, Fakhr, I.M., Elwahy, A.H.M., Awad, H.M. Synthesis and in vitro evaluation of novel tetralin-pyrazolo[3,4-b]pyridine hybrids as potential anticancer agents *J. Heterocycl. Chem*., 2020, 57, 182–196.

[7] Hamza, E.K., Hamdy, N.A., Zarie, E.S, Fakhr, I.M., Elwahy, A.H.M., Awad, H.M. Synthesis and in vitro anticancer evaluation of novel pyridine derivatives bearing tetrahydronaphthalene scaffold. *Arkivoc*, 2019, 2019, 459–480.

[8] Gamal-Eldeen, A.M., Hamdy, N.A., Abdel-Aziz, H.A., El-Hussieny, E.A., Fakhr, I.M.I. Induction of intrinsic apoptosis pathway in colon cancer HCT-116 cells by novel 2-substituted-5,6,7,8-tetrahydronaphthalene derivatives. *Eur. J. Med. Chem*., 2014, 77, 323–333.

[9] Hamdy, N.A., Anwar, M.M., Abu-Zied, K.M., Awad, H.M. Synthesis, tumor inhibitory and antioxidant activity of new polyfunctionally 2-substituted 5,6,7,8-tetrahydronaphthalene derivatives containing pyridine, thioxopyridine and pyrazolopyridine moieties. *Acta Poloniae Pharmaceutica,* 2013, 70, 987–1001.

[10] Hamdy, N.A., El-Senousy, W.M., Fakhr, I.M.I. Enaminone as building blocks in organic chemistry: A novel route to polyfunctionally 2-substituted 5,6,7,8-tetrahydronaphthalenes and their antiviral evaluation. *J. Heterocycl. Chem*., 2013, 50, 337–343.

[11] Bekheit, M.S., Mohamed, H.A., Abdel-Wahab, B.F., Fouad, M.A. Design and synthesis of new 1,4,5-trisubstituted triazole-bearing benzenesulphonamide moiety as selective COX-2 inhibitors. *Med. Chem. Res*., 2021, 30, 1125–1138.

[12] Kariuki, B.M., Abdel-Wahab, B.F., El-Hiti, G.A. Synthesis and structural characterization of isostructural 4-(4-aryl)-2-(5-(4-fluorophenyl)-3-(1-(4-fluorophenyl)-5-methyl-1H-1,2,3-triazol-4-yl)-4,5-dihydro-1H-pyrazol-1-yl)thiazoles. *Crystals*, 2021, 11, 795.

[13] Sert, Y., El-Hiti, G.A., Gökce, H., Abdel-Wahab, B.F., Kariuki, B.M. DFT, molecular docking and experimental FT-IR, laser-Raman, NMR and UV investigations on a potential anticancer agent containing triazole ring system. *J. Mol. Struct*., 2020, 1211, 128077.

[14] Abuelizz, H.A., Marzouk, M., Bakheit, A.H.,Awad, H.M., Soltan, M. M., Naglah, A.M., Al-Salahi, R. Antiproliferative and antiangiogenic properties of new VEGFR-2-targeting 2-thioxobenzo[g]quinazoline derivatives (In Vitro). *Molecules*, 2021, 25(24), 5944.

[15] Awale M., Reymond J.L., The polypharmacology browser: a web-based multi-
[16] prediction tool using ChEMBL bioactivity data. J. Chem., 2017, 9, 11.
[17] Bouattour M., Raymond E., Qin S., Cheng A.L., Stammberger U., Locatelli G., Faivre S. Recent developments of c-Met as a therapeutic target in hepatocellular carcinoma. *Hepatology*., 2018, 67, 1132–1149.
[18] Bourton E.C., Ahorner P.A., Plowmn P.N., Zahir S.A. , Al-Ali H., Parris C.N. The PARP-1 inhibitor Olaparib suppresses BRCA1 protein levels, increases apoptosis and causes radiation hypersensitivity in BRCA1 +/- lymphoblastoid cells. *J. Cancer.*, 2017, 8, 4048–4056.
[19] Cui J.J., Tran-Dubé M., Shen H., Nambu M., Kung P.P., Pairish M., Jia L., Meng J., Funk L., Botrous I., McTigue M., Grodsky N., Ryan K., Padrique E., Alton G., Timofeevski S., Yamazaki S., Li Q., Zou H., Christensen J., Mroczkowski B., Bender S., Kania R.S., Edwards M.P. Structure based drug design of Crizotinib (PF-02341066), a potent and selective dual inhibitor of mesenchymal–epithelial transition factor (c-MET) Kinase and Anaplastic Lymphoma Kinase (ALK). *J. Med. Chem*., 2011, 54, 6342– 6363.
fingerprint target
[20] Dawicki-McKenna J.M., Langelier M.F., DeNizio J.E., Riccio A.A., Cao C.D., Karch K.R., McCauley M., Steffen J.D., Black B.E., Pascal J.M. PARP-1 Activation Requires Local Unfolding of an Autoinhibitory Domain. *Mol. Cell*., 2015, 60, 755–768.
[21] Morris G.M., Huey R., Lindstrom W., Sanner M.F., Belew R.K., Goodsell D.S., Olson A.J. AutoDock4 and AutoDockTools4: Automated docking with selective receptor flexibility. *J Comput Chem*.,2009, 30, 2785–2791.
[22] Trott O., Olson A.J. AutoDock Vina: improving the speed and accuracy of docking with a new scoring function, efficient optimization, and multithreading. *J. Comput. Chem.*, 2010, 31, 455–461.
[23] Salentin S., Schreiber S., Haupt V.J., Adasme M.F., Schroeder M. PLIP: fully automated protein-ligand interaction profiler. *Nucl. Acids Res*., 2015, 43, W443-W447.
[24] DeLano, W. L., the PyMOL Molecular Graphics System; DeLano Scientific: San Carlos, CA, 2002(2009).
[25] Laskowski R A, Swindells M B. LigPlot+: multiple ligand-protein interaction diagrams for drug discovery. *J. Chem. Inf. Model*., 2011, 51, 2778-2786.